

Direct mechanical measurement of geodesic structures in rat mesenchymal stem cells

P. Maguire,^{1,2,a)} J. I. Kilpatrick,^{1,a)} G. Kelly,^{1,2} P. J. Prendergast,^{1,2}
V. A. Campbell,^{1,2} B. C. O'Connell,^{1,2} and S. P. Jarvis^{1,a)}

¹Centre for Research on Adaptive Nanostructures and Nanodevices (CRANN), Trinity College Dublin, Dublin 2, Ireland

²Trinity Centre for Bioengineering, School of Engineering, Trinity College Dublin, Dublin 2, Ireland

(Received 1 February 2007; accepted 23 August 2007; published online 19 September 2007)

During numerous biological processes, cell adhesion, cell migration and cell spreading are vital. These basic biological functions are regulated by the interaction of cells with their extracellular environment. To examine the morphology and mechanical changes occurring in mesenchymal stem cells cultured on a mechanically rigid substrate, atomic force microscopy and fluorescence microscopy were employed. Investigations of the cells revealed both linear and geodesic F-actin configurations. No particular cell characteristics or intra-cellular location were implicated in the appearance of the geodesic structures. However, the length of time the cells were cultured on the substrate correlated with the percentage appearance of the geodesic structures. Calculating energy dissipation from cell images acquired by dynamic mode atomic force microscopy, it was observed that the vertices of the geodesic structures had significantly higher energy dissipation compared to the linear F-actin and the glass. This supports work by Lazarides [*J. Cell Biol.* 68, 202–219 (1976)], who postulated that the vertices of these geodesic structures should have a greater flexibility. Our results also support predictions based on the microfilament tensegrity model. By understanding the basic principles of cell ultrastructure and cell mechanics in relation to different extracellular environments, a better understanding of physiological and pathological process will be elicited. [DOI: 10.2976/1.2781618]

CORRESPONDENCE

P. Maguire: p.maguir@ucd.ie
P. J. Prendergast: pprender@tcd.ie
S. P. Jarvis: suzi.jarvis@ucd.ie

During numerous biological processes, such as bone remodeling and wound healing, cell adhesion, migration and spreading are vital processes. These basic biological functions are regulated by the interaction of the cells with their extracellular environment. Chemical characteristics, mechanical integrity and the spatial and topographical organization of the extracellular environment have all been reported to influence cell function (Snaidecki *et al.*, 2006). Surface topography and surface chemistry have been extensively studied in the literature. In relation to surface topography

Lim *et al.* (2005) reported that osteoblast cells cultured on a textured surface with nanoscale islands display a significant increase in cell spreading, adhesion and proliferation compared to flat surfaces or surfaces with larger islands. Reporting on surface chemistry, Takai *et al.* (2005 and 2006) reported that osteoblast cells cultured on substrates coated in fibronectin display a significant increase in their elastic modulus and responsiveness to flow. Despite a growing literature on cell-substrate interactions, less is known about how cells sense the mechanical integrity of their extracellular environment. Early work in this area utilized hydrogels of variable stiffness, which was controlled by varying the cross-linking densities (Wang and Pelham, 1998; Pelham and Wang, 1997). Lo *et al.*, 2000 reported that fibroblast cells

^{a)}New Address for P. Maguire, J. I. Kilpatrick and S. P. Jarvis, UCD Conway Institute of Biomolecular & Biomedical Research, University College Dublin, Belfield, Dublin 4.

cultured on a mechanically rigid extracellular environment displayed a broad and flatter morphology compared to fibroblasts grown on an equally adhesive mechanically softer substrate. These authors also reported that fibroblasts actively migrate from a mechanically soft substrate to a more mechanically rigid substrate. The above observations have been reported to occur in multiple cell types from fibroblasts to neurons and on a wide variety of surfaces differing only in mechanical integrity (see [Wong et al., 2004](#) for a review).

In relation to biological processes *in vivo*, any modification of the interface between the extracellular environment and the cell can induce and promote adverse cellular effects. For example, atherosclerosis has been reported to involve the remodeling of the surrounding extracellular environment ([Hayashi and Imai, 1997](#); [Matsumoto et al., 2002](#)). Remodeling of the extracellular environment in the early stages of this disease is marked by a lesion which is softer than the surrounding tissue. As the disease progresses, a fibrous and calcified cap forms in the lesion area which has a significantly higher stiffness compared to the surrounding normal healthy tissue. This remodeling of the extracellular environment leads to the accumulation of “unwanted” vascular smooth muscle cells, resulting in narrowing of the arteries. Changes in the mechanical properties of the extracellular environment have also been observed in the study of oncology where softer extracellular matrices have been observed to be more efficient at promoting tubulogenesis ([Deroanne et al., 2001](#)). *In vitro* studies in the field of regenerative medicine ([Engler et al., 2006](#)) have shown that collagen I expression in Mesenchymal Stem Cells (MSCs) is low when MSCs are cultured on a soft extracellular matrix with a mechanical integrity of <11 kPa but was significantly higher when the MSCs were cultured on an extracellular matrix with a mechanical integrity of 34 kPa. These results suggest that the mechanical integrity of the biomaterial employed as a substrate for the purposes of MSC culture can actually influence stem cell differentiation. These examples illustrate the importance of understanding how cells interact with their extracellular matrix if we wish to be able to control a range of physiological and pathological process.

The cytoskeleton, the cell’s mechanical scaffold, is a dynamic, highly conserved and structured network of proteins composed of actin microfilaments, microtubules and intermediate filaments. The cytoskeleton has been observed using an array of imaging techniques such as scanning electron microscopy and fluorescent microscopy. In order to study the subcellular structure of MSCs we employed atomic force microscopy (AFM) ([Binnig et al., 1986](#)) as it can be used to investigate dynamic responses of the cell, as well as the cell’s nanomechanical properties at highly localized positions across the cell, under physiological conditions ([Hofmann et al., 1997](#); [Radmacher et al., 1994](#); [Henderson et al., 1992](#)). This is achievable via AFM by the precise application and monitoring of highly localized forces between a sharp tip and

the cell of interest. The tip is mounted on a cantilever, the deflection of which is detected in order to extract force from its displacement via Hooke’s law. The most common deflection detection system involves monitoring the position of a laser beam reflected from the backside of the cantilever onto a segmented photodiode.

Our study investigates MSCs, which are multipotent mechanosensitive cells capable of generating multiple stromal cell lineages such as osteoblasts, adipocytes, chondrocytes and myocytes ([Pittenger et al., 1999](#)). The efficiency of MSC’s isolation from the bone marrow, combined with the fact that MSCs are easily expanded *in vitro* ([Burder et al., 1997](#)) makes MSCs a prime candidate for application in tissue engineering and regenerative medicine. MSCs have been reported to be able to circulate away from their niche in the bone marrow, engrafting and hence differentiating on a range of different extracellular environments. Therefore, it is important to understand the effect of the physical attributes of the extracellular environment (both on the micro and nanoscale) on the biological function of MSCs.

In this manuscript, employing AFM and fluorescence microscopy, we have investigated and mechanically characterized *in situ* the subcellular structure of rat MSCs (rMSCs) cultured *in vitro* on a mechanically rigid substrate over time. We have observed the formation of geodesic F-actin structures, which differ significantly in their mechanical properties from the traditionally viewed and studied linear F-actin. The presence of geodesic structures was observed to correlate only with the length of time seeded on the substrate. By exploring the interactions of MSCs with their substrate over time, we will be able to further our understanding of changes in cell morphology and phenotype as a result of interactions with the extracellular environment.

MATERIALS AND METHODS

Cell isolation and cell culture of rat MSCs (rMSCs)

The rMSCs were isolated from the femur and tibia of adult male Wistar Rats using the classical plastic adherence method developed by [Friedenstein et al. \(1976\)](#). Briefly, the femur and tibia were removed and surrounding soft tissue carefully removed. The bones were placed in sterile Dulbecco’s modified eagles medium (Sigma-Aldrich, Dorset, U.K.) supplemented with 10% fetal bovine serum (Gibco, Paisley, U.K.), 2 mM L-glutamine (Gibco, Paisley, U.K.), 1% penicillin streptomycin (Gibco, Paisley, U.K.) and 1% amino acids (Gibco, Paisley, U.K.). The epiphyses of the bones were removed and the bone marrow flushed out of the bone with supplemented culture medium, drawn and expelled with a syringe 12, 16 and 20 gauge (Sigma-Aldrich, Dorset, U.K.), respectively, three times. The remaining supernatant was placed in a plastic petri dish and placed in an incubator at 37 °C for 30 min. The supernatant was then removed and placed in a T25 culture flask (NUNC, Uden, Denmark). The rMSCs were kept in an incubator at 37 °C with 95% humid-

ity and 5% CO₂. Subculture was routinely performed at ~80% confluence, using 0.25% trypsin (Sigma-Aldrich, Dorset, U.K.). After three weeks culture the rMSCs were employed for experiments.

LIVE CELL IMAGING

rMSCs were seeded on an untreated glass substrate and incubated for 2 h to facilitate attachment to the substrate. The cells were then placed on a Zeiss Cell Observer for 72 h and a phase contrast image acquired every 10 min using a Zeiss 10x objective lens with a numerical aperture of 0.03. During the acquisition of the live cell imaging, cells were maintained at 37 °C with 95% humidity and 5% CO₂. In order to prevent unnecessary exposure of the cells to high light intensity during the acquisition of the image, the light intensity was set low and the image contrast enhanced after experiment completion.

CD 90 staining

CD90 is a positive surface marker for MSCs (Kici *et al.*, 2003, Rochefort, 2005). rMSCs were seeded at low-medium density on 22 mm² glass substrates and maintained under appropriate cell culture conditions. After 24 h rMSCs were prewashed twice in prewarmed 1X phosphate buffered saline (PBS) (Sigma-Aldrich, Dorset, U.K.), pH 7.4, and fixed in 4% paraformaldehyde (Sigma-Aldrich, Dorset, U.K.) for 20 min at room temperature. The paraformaldehyde solution was then removed and cells washed twice in 1X Tris Buffered Solution (TBS) (10 X Tris buffer=31.52 g Tris HCL and 87.66 g NaCl made up in 1 l distilled water, pH 7.4) (TBS). Nonreactive sites were blocked for 2 h at room temperature using a blocking buffer [2% Bovine Serum Albumine (BSA) in 1X TBS with 0.1% Triton X100 (Sigma-Aldrich, Dorset, U.K.) and 20% heat-inactivated horse serum (Gibco BRL, Ireland)]. The cells were then washed in 1X TBS. A 1:500 dilution of the mouse monoclonal primary antibody, CD90 (Abcam, Cambridge, U.K.), made up in blocking buffer, was added. Cells were left in a humidified chamber overnight. Cells were then washed three times in 1X TBS and incubated for 1 h with a 1:50 biotinylated goat anti-mouse IgG secondary antibody (Abcam, Cambridge, U.K.) made up in blocking buffer. Cells were then washed in 1X TBS three times. A 1:50 ExtrAvidin FITC solution, made up in 1X TBS, was incubated with the cells at room temperature in the dark for 1 h. ExtrAvidin FITC is a tetrameric protein conjugated to fluorescein isothiocyanate (FITC) and is commonly used in fluorescent biotin avidin techniques in immunocytochemistry due to its high sensitivity and highly efficient detection system. The negative control received no primary antibody and was left incubating overnight in blocking buffer. This was carried out in order to calculate the background fluorescence intensity caused by nonspecific binding of the ExtrAvidin FITC solution. The cells were then washed in distilled water and mounted using Vectashield (Vector,

California, USA). Confocal microscopy cells were excited at 488 nm and emission recorded using a long pass filter at 505 nm. The fluorescence intensity of 900 cells per run (i.e., 900 cells per n , 2700 for $n=3$, where each n is from a separate rat) were quantified.

F-actin staining

rMSCs were seeded on 22 mm² glass substrates at a low to medium density. rMSCs were maintained under appropriate cell culture conditions for the duration of the respective experiments. rMSCs were prewashed twice in prewarmed 1X PBS and fixed in 4% paraformaldehyde for 20 min at room temperature. The paraformaldehyde was then removed and cells washed in 1X PBS twice. The cells were then exposed to pure acetone for 5 min at -20 °C. The cells were then washed in 1X PBS and incubated at room temperature in the dark for 30 min with one unit of phalloidin, fluorophore Oregon Green 514 phalloidin (Molecular Probes, Leiden, Netherlands). Phalloidin is isolated from the deadly Amanita phalloide mushrooms and is commonly used for staining F-actin in fixed cells and tissues (Wieland, 1986). One unit of phalloidin was equivalent to 5 μ l of methanolic stock solution, which was made up in 200 μ l 1X PBS. The dye was then removed and the cells washed in 1X PBS. The samples were then loaded into custom designed holders. The fluorophore was excited at ~510 nm and emission recorded at ~530 nm. With the samples coded, to keep the identity of the sample unknown from the experimentalist, 900 cells were counted and scored as having F-actin hexagonal arrays (geodesic units) or not where $n=3$ (i.e., 900 cells per n , 2700 for $n=3$, where each n is from a separate rat). The appearance of the hexagonal F-actin arrays in cells was expressed as a percentage of the total population counted. In order to quantify the fluorescence intensity of the vertices versus the interconnecting F-actin structures in the geodesic units, the areas of interest were highlighted, and using Zeiss software, the fluorescence intensity recorded.

Imaging F-actin and CD90 simultaneously

Samples were stained for Oregon Green 514 and CD90 as described above. CD90 and Oregon Green 514 have emission regions which overlap, thus "cross talk" between these two fluorophores exists. To overcome this, a Zeiss confocal META system was employed. This system permits fluorophores with emission in the same region to be unmixed. Samples were first stained with Oregon Green 514 or CD90 alone. The samples were then excited and emission spectra created for each and saved. A sample was then stained for both CD90 and Oregon Green 514. The sample was then excited and the emission spectra collected. Using the reference spectra for CD90 and Oregon Green 514, their emissions could then be unmixed.

AFM SETUP AND CALIBRATION

Cell conditions for AFM imaging

The culture medium was removed prior to AFM imaging. The cells were washed and imaged in sterile 1X PBS. Imaging was carried out on live rMSCs seeded on an uncoated glass slide at room temperature. All cells were kept on the AFM stage for a maximum duration of 2–3 h. Cells were imaged by the AFM at a constant scan rate of 0.5 Hz.

Experimental design for Dynamic Mode AFM

The sample holder containing the cells was placed on the AFM scanner (Asylum MFP-3D Bio, California) directly above the objective lens of the inverted optical microscope. In this position, the AFM cantilever could be observed through the objective lens. The AFM cantilevers employed for imaging were rectangular NSC36 cantilevers with a stiffness range from 0.5 to 2.5 N/m (Mikromasch, Germany). The stiffness and sensitivity of the cantilevers was calibrated (as described below), both in air and in 1X PBS. The level of the AFM head was then lowered such that the tip lies several millimeters above the sample. The cantilever was brought to the substrate by engaging in contact mode, meaning that any cantilever deflection during advancement towards the cell membrane was controlled in a feedback loop that maintains deflection at a predetermined “setpoint” value via appropriate displacement of the base of the cantilever via a piezo. This ensures a “soft landing.” The height of the tip was then adjusted to $>5 \mu\text{m}$ above the glass substrate ensuring that the tip was at least $2 \mu\text{m}$ above any rMSC. The conical tip was then placed above a region of the rMSC cell.

Quantifying the applied force

To determine the magnitude of force applied to the rMSC membrane by deflection of the AFM tip, it was necessary to determine (i) the stiffness of the cantilever, and (ii) the sensitivity of the deflection detection system. This was done prior to each experiment, using the methods described below, initially in air and then again once the cantilever was immersed in 1X PBS.

- (i) The method used to determine the stiffness (k) is based on an expression derived by Sader (1998) for a long rigid beam with a rectangular cross section. The expression [Eq. (1) below] relates k to: the rectangular dimensions of the cantilever (L and b); fluid density (ρ); resonant frequency of oscillation (ω_f); quality factor (Q_f) of the resonant peak; and Γ_i^f , a function of the fluid hydrodynamics (based on the velocity field, hydrodynamic pressure, density and viscosity of the fluid).

$$k = 0.1906\rho b^2 L Q_f \omega_f^2 \Gamma_i^f(\omega_f) \quad (1)$$

The “Sader” method has been experimentally validated (Chon *et al.*, 2000), and is accurate provided that the length of the cantilever greatly exceeds its

width, which in turn must exceed its thickness, and that the quality factor significantly exceeds unity. The plan view dimensions of the rectangular cantilever were taken from the manufacturer’s specifications. The resonant frequency and quality factor were determined from the thermal spectrum, i.e., the cantilever oscillations due to thermal noise in the liquid medium. The method is less accurate for a cantilever in liquid than in air as the resonant peak is less pronounced and the quality factor lower. However, a prerequisite for proceeding with each experiment was that stiffness values obtained both in air and liquid did not vary by more than $\sim 10\%$.

- (ii) The sensitivity of the deflection detection system (in nm/V), i.e., the deflection corresponding to the measured photodiode voltage, was also determined from thermal spectra for each cantilever using the method described by Higgins *et al.* (2006).

Calculation of energy dissipation

In dynamic mode (tapping mode) AFM the cantilever is driven with a signal of fixed radial frequency, ω_D and amplitude A_D . At large separations, where there are no surface forces acting, the motion of the cantilever can be described by a free oscillation amplitude, A_0 , and a phase, φ . As the tip-sample separation is reduced, the surface forces influence the cantilever oscillation amplitude, A , and phase. Imaging is then performed using a feedback loop to maintain the condition of $A = A_{SP}$, where A_{SP} is the amplitude setpoint, by varying the tip-sample distance while simultaneously acquiring the phase signal.

Assuming that the ω_D is chosen to be the resonant frequency, ω_0 , and that $A_0 = Q A_D$, where Q is the quality factor, the energy dissipated during tip-sample interactions, \bar{P}_{tip} can be calculated using Eq. (2) (Anczykowski *et al.*, 1999).

$$\bar{P}_{tip} = \frac{1}{2} \frac{k\omega_0}{Q} [A_0 A \sin \varphi - A^2] \quad (2)$$

where k is the spring constant.

All calculations of energy dissipation presented here have been normalized such that the free lever amplitude A_0 is set equal to the setpoint amplitude for imaging, A_{SP} . Under experimental conditions, whether or not the actual lever amplitude A is equal to the setpoint amplitude A_{SP} , at any point in the image, is dependent upon instrumental factors including feedback loop bandwidth and tip velocity. Since it was observed that this condition was not always met in our images, the actual measured value of A at each point was included in the energy dissipation evaluation and we thus present our findings in terms of qualitative values of relative energy dissipation where comparison is valid within a single image.

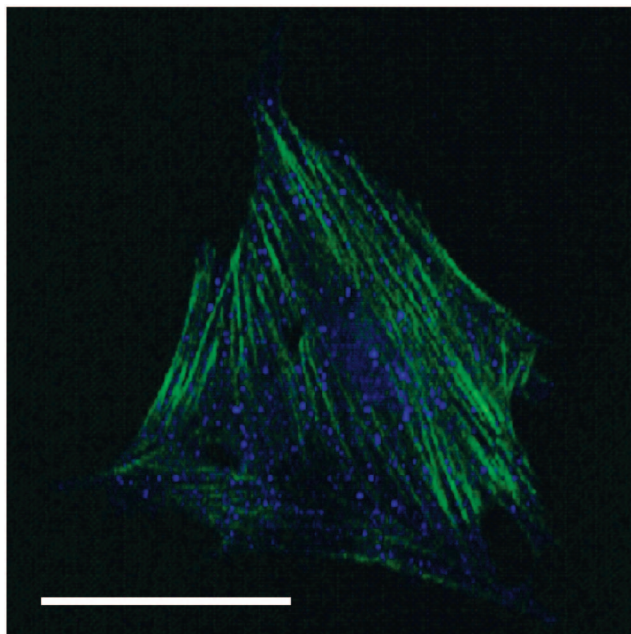


Figure 1. rMSCs stained with Oregon Green 514 for F-actin (Green) and CD90 (Blue), a positive marker for rMSCs. Linear filaments represent the F-actin and the punctate staining represents the spread of CD90 receptors on the surface of the cell.

Monitoring cell membrane viability

Propidium Iodide (PI) (Sigma-Aldrich) is a membrane impermeable dye; therefore it can only pass through the cell membrane into the cell if there is a loss in cell membrane integrity (Smolewski *et al.*, 2002). Once in the cell, PI binds to nuclei acid molecules. rMSCs were seeded at low densities on glass coverslips, diameter 40 mm, and incubated in culture medium until the cells had attached. The medium was then removed and 5 ml of culture medium was added and left overnight at 37 °C. The culture medium was removed and the cells were washed with 1X PBS buffer. rMSCs were loaded with 1 μ l/ml of PI in 1X PBS and incubated with the cell while carrying out AFM and combined fluorescence microscopy. PI excitation and emission was monitored at 580 and 630 nm, respectively.

Statistics

Significance was determined by a student's unpaired *t* test, and the differences were considered significant if $P \leq 0.05$.

RESULTS AND DISCUSSION

The interaction of cells with their extracellular environment is known to induce many physiological and pathological processes *in vivo* (Hayashi and Imai, 1997; Matsumoto *et al.*, 2002; Deroanne *et al.*, 2001). Using AFM and combined fluorescence microscopy we report the *in situ* mechanical properties of adherent primary rMSCs cultured *in vitro*. F-actin geodesic structures were observed hence providing evidence supporting the microfilament tensegrity model

for cell mechanics and the mechanical theory proposed by Lazarides (1976) based on the spatial distribution of tropomyosin and myosin in the cell.

Employing the protocol for rMSC isolation of Friedenstein *et al.* (1976), using confocal microscopy it was observed that cells isolated from the femur and tibia of adult rats and plated on a glass substrate stained positive for CD90, a positive surface marker for rMSCs (Kici *et al.*, 2003; Jiang *et al.*, 2006) (Fig. 1). Using this protocol for rMSC isolation and employing leukocytes as a negative control for CD90 expression, work from our group characterized the rMSC population as $96.9 \pm 0.4\%$ positive for CD90^b. Carrying out live cell imaging on adherent rMSCs under physiology conditions for 72 h we observed significant morphological changes (Fig. 2). Following 10 rMSCs over 72 h, rMSCs increased in cell diameter from $\sim 20 \mu\text{m}$ to $> 110 \mu\text{m}$ with rMSCs observed to display a high ratio of cytoplasm to nucleus (Fig. 2). These observations indicate that a significant change in cell morphology occurs as result of the interaction of the rMSCs with their untreated glass substrate. These results support work by Lo *et al.*, 2000 and the mechanical model of tensegrity (Ingber and Jamieson, 1985). The tensegrity model states that the cytoskeleton generates a level of tension by pulling against the extracellular environments in a manner which is proportional to the extracellular environment's stiffness, thus, generating the above morphological characteristics.

When imaging with AFM, the tip is in direct contact with the sample. Depending on the magnitude of the force, the cell's subcellular structure may also be investigated. This is due to the deformation of the membrane around and on top of the subcellular structures. In principle, the higher the force the deeper the sampling depth into the cell and the more subcellular detail obtained. However, as the force is increased the probability of damaging the cell also increases. For this reason the inclusion of an independent control to monitor membrane viability is necessary. In this experiment, PI was employed to monitor cell membrane viability during AFM imaging and it was observed that the forces applied for AFM imaging did not compromise membrane integrity. Figure 3 represents an image acquired using dynamic mode AFM. In this image the long linear filaments of the subcellular structure can be observed.

Images acquired using dynamic mode AFM of rMSCs seeded on glass revealed hexagonal subcellular structures (Fig. 4). It was observed that six subcellular filaments appeared to radiate from/to a central node (or vertices), hence forming a geodesic network (Fig. 4). Employing fluorescence microscopy, it was observed that the geodesic structures observed by AFM imaging stained positive for Oregon Green 514, a fluorophore for F-actin (Fig. 5). Quantifying

^bChondrogenic differentiation of MSCs in a collagen-GAG scaffold: experimental and computational analysis. McMahon, L, Reid, A. J., Campbell, V. A. and Prendergast, P. Submitted to *Annals for Biomedical Engineering*.

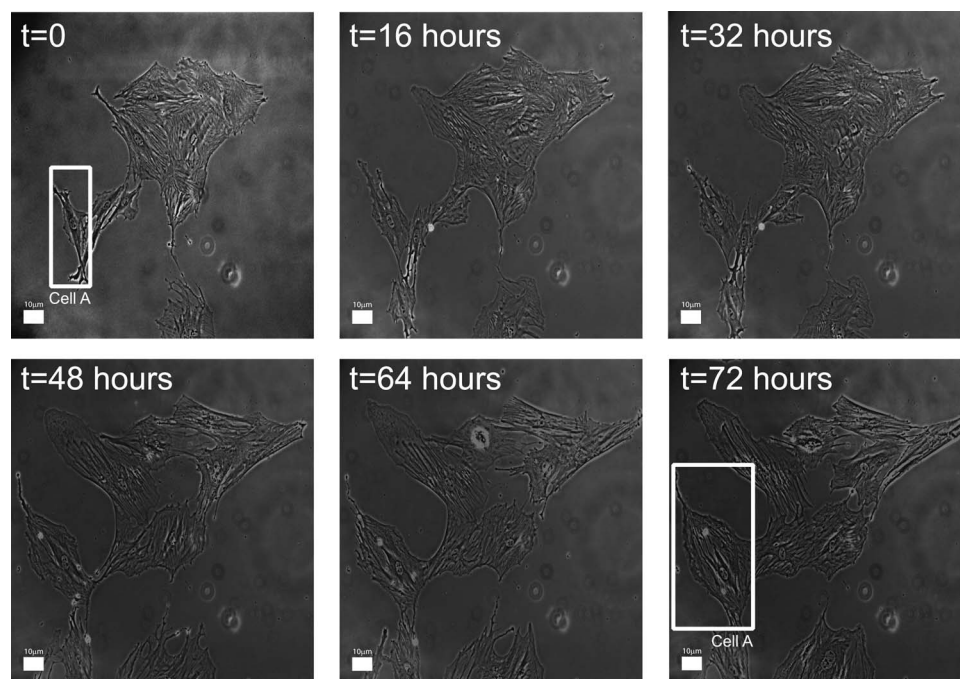


Figure 2. Live cell imaging of 10 rMSCs over 72 h under physiological conditions; t=0 represents the start of the experiment, 2 h after the cells were plated. A white box is drawn around a single cell (cell A) in the first and last time frame.

the appearance of these structures in rMSCs, it was observed that (1) no correlation existed in the cellular location of these structures, (2) significant variation in the development of the geodesic structures existed, (3) geodesic structures occurred in isolated single cells as well as in cells within a confluent cell layer, and (4) it was observed that the percentage of cells exhibiting geodesic structures in rMSCs was dependent on the length of time seeded on the glass substrate (Fig. 6). F-actin geodesic configurations have been observed in multiple cell lines using fluorescent microscopy and more recently in permeabilized and fixed cells using contact mode AFM under dry conditions (Lazarides and Weber, 1974; Lazarides, 1976; Osborne *et al.*, 1978; Heuser and Kirschner, 1980; Miller and Theiss, 2005). Referring to geodesic structures Fuller (1965) stated that tension dependent structures gain their stability by “triangulating” their internal supporting elements. According to Ingber *et al.* (1993) these struc-

tures can be explained solely using the mechanical assumptions of the tensegrity model, with the development of these geodesic structures depending on many factors, which include the level of cytoskeleton tension, mechanical integrity of the cell, cell shape and size of the cell nucleus.

The appearance of F-actin geodesic structures has been observed in multiple cell lines using fluorescence microscopy; however no *in situ* mechanical data on these structures exist to our knowledge. To further our understanding of these structures and to investigate any mechanical differences occurring between the linear F-actin and the F-actin vertices, energy dissipation was calculated from the phase and amplitude traces acquired during dynamic force AFM. This created a relative energy dissipation map of the cell (a measure of energy that is transferred from the tip during the interaction with the sample). Although, as discussed in the method section, there are quantitative limitations to this formula,

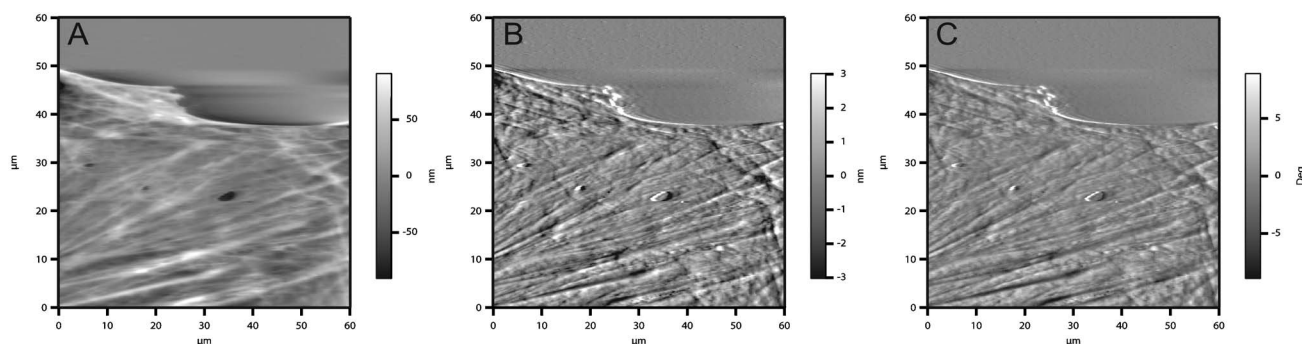


Figure 3. 60 μm^2 of a single live rMSC acquired by Dynamic Mode AFM. (A) Height trace, (B) amplitude trace, (C) phase trace. Scan rate 0.5 Hz

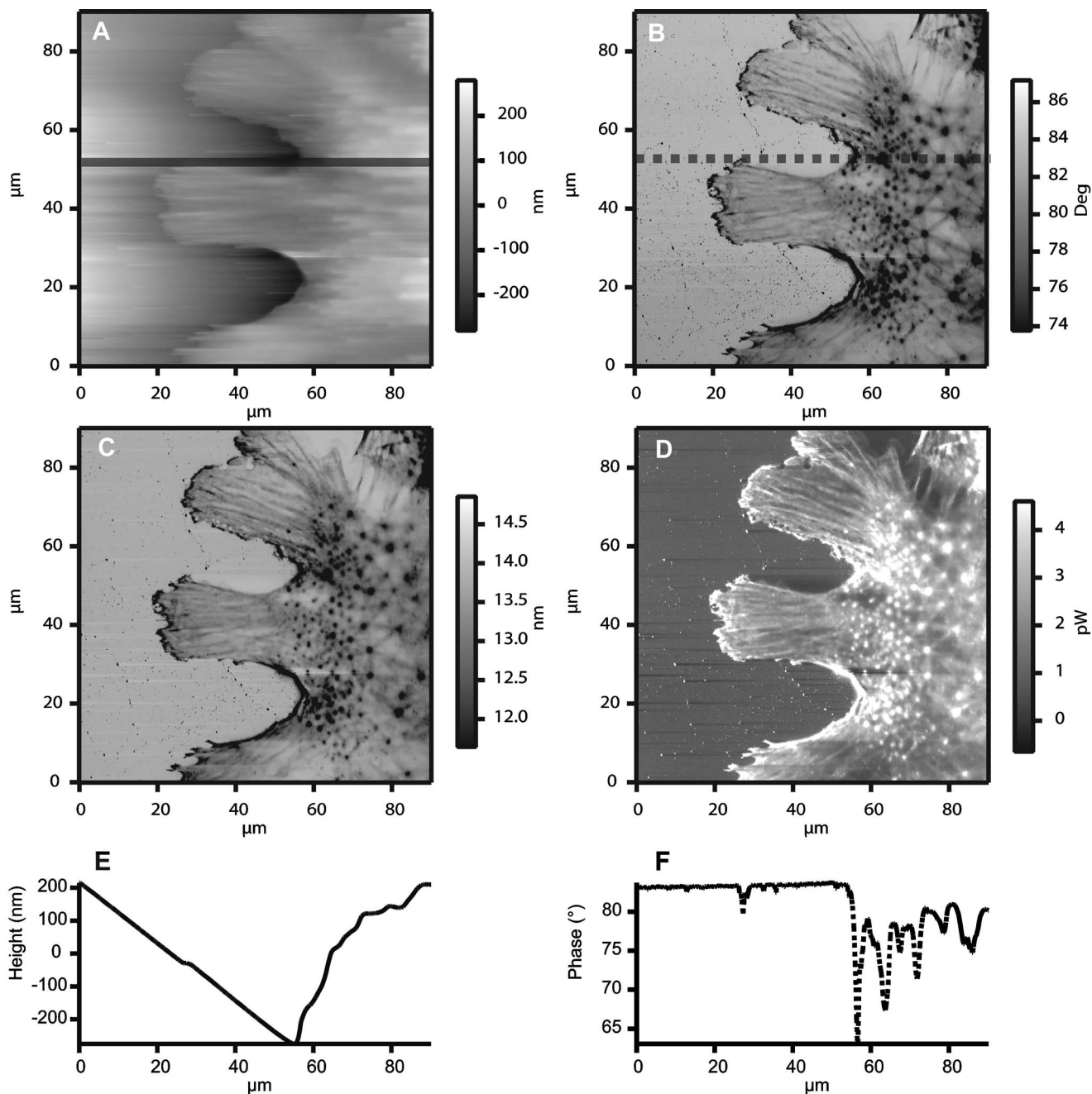


Figure 4. $90 \mu\text{m}^2$ of a single live rMSC acquired by Dynamic Mode AFM. (A) Height trace, (B) amplitude trace, (C) phase trace, and (D) energy dissipation. Scan rate 0.5 Hz. For calculation of (D), the dissipation map, $k=6.0 \text{ N m}$, resonance frequency=59,060 Hz, quality factor=5.4, setpoint amplitude=13.76 nm and drive frequency 58,132 Hz, (E) average height trace of ten scan lines across the cell. A first order flattening was applied to the image, therefore the observed slope on the height trace across the glass is an artifact of the imaging processing, (F) average phase change of ten scan lines across the cell.

qualitative results are possible, permitting relative comparison between different cellular regions. It should be noted that the high dissipation at the peripheral cellular regions is an artifact of the increase in contact area at the glass-cell interface (Nagao and Dvorak, 1999). The relative energy dissipation map indicates a significant increase in energy dissipation at the central vertices of the geodesic structures

compared to the linear F-actin filaments and the glass substrate.

Topographical changes in a sample can induce changes in energy dissipation as observed at the periphery of the cell. Therefore, this influence on energy dissipation must be considered. As can be observed from Fig. 4(A), due to the sample size, velocity of the tip and the feedback bandwidth,

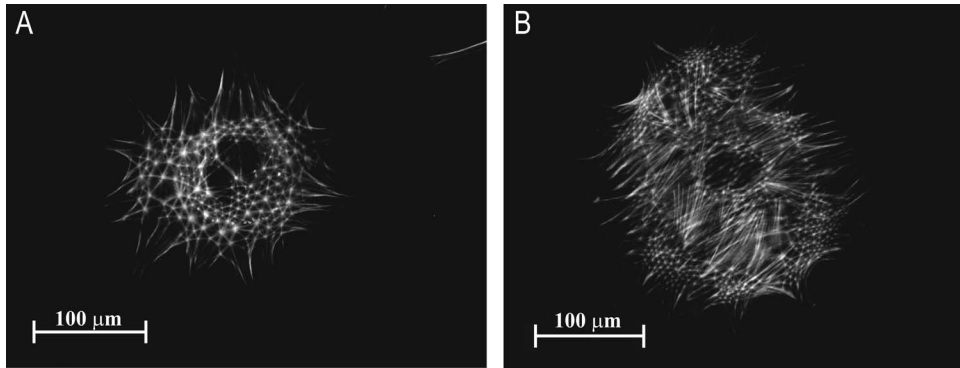


Figure 5. F-actin in rMSCs stained with Oregon Green 514.

the height trace was at low resolution. Figure 7 illustrates an accurate height trace across actin filaments taken over a much smaller area; here the feedback bandwidth was sufficient to follow the surface contours. Thus, a correlation can be made between height and phase shifts across actin filaments in Fig. 7 and Fig. 4. Energy dissipation calculated from Fig. 7 illustrates that the energy dissipation across linear F-actin filaments, in this case, was similar to that observed in Fig. 4. Therefore, we do not consider that topographical changes make a significant contribution to the increase in energy dissipation across the F-actin vertices in the geodesic structures.

An increase in energy dissipation can originate under two additional circumstances. The first is a change in the surface chemistry resulting in adhesion between the tip and the surface. The second is a change in the mechanical properties of the cell. Hence, we needed to investigate further to elicit if the increase in dissipation energy at the vertices was due to either chemistry or mechanical integrity. If the observed increase in energy dissipation could be attributed to mechani-

cal properties then this would mean that the vertices are more flexible compared to the surrounding F-actin. The reasoning for such a correlation is that the extent of energy loss is proportional to the deformation volume, i.e., a low flexibility substrate will undergo relatively small deformation as the volume of elastic and plastic fields under the AFM tip is small. A very flexible substrate will undergo high deformation as there are large elastic and plastic fields under the AFM tip. If, however, the increase in energy dissipation was due to a change in chemistry then the relative dissipation map would indicate that the vertices have higher adhesion than the surrounding cell membrane. Naogao and Dvorak (1999) postulated that adhesion forces may be significantly reduced in fluid. This postulation was based on their observation that in vertebrate cells phase shift transitions are not affected by changes in the tapping force. They therefore state that a shift in phase is the result of stiffness or the viscoelastic properties of the cell.

Using fluorescence microscopy we observed that when rMSCs were stained for F-actin the vertices of the geodesic

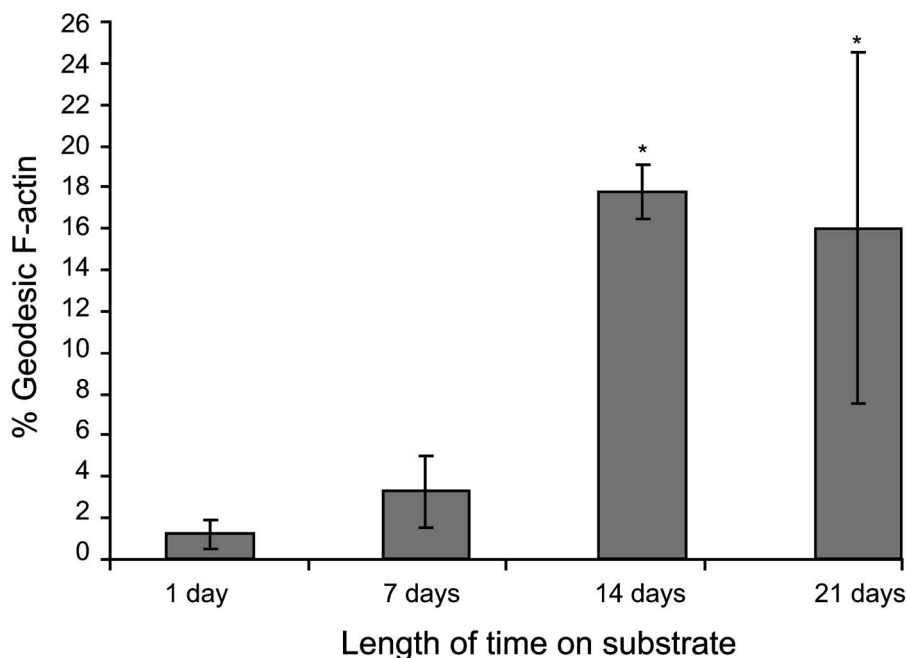


Figure 6. Percentage expression of geodesic F-actin structures observed in rMSCs plated on a glass substrate over 21 days. $n=3 * p \leq 0.05$.

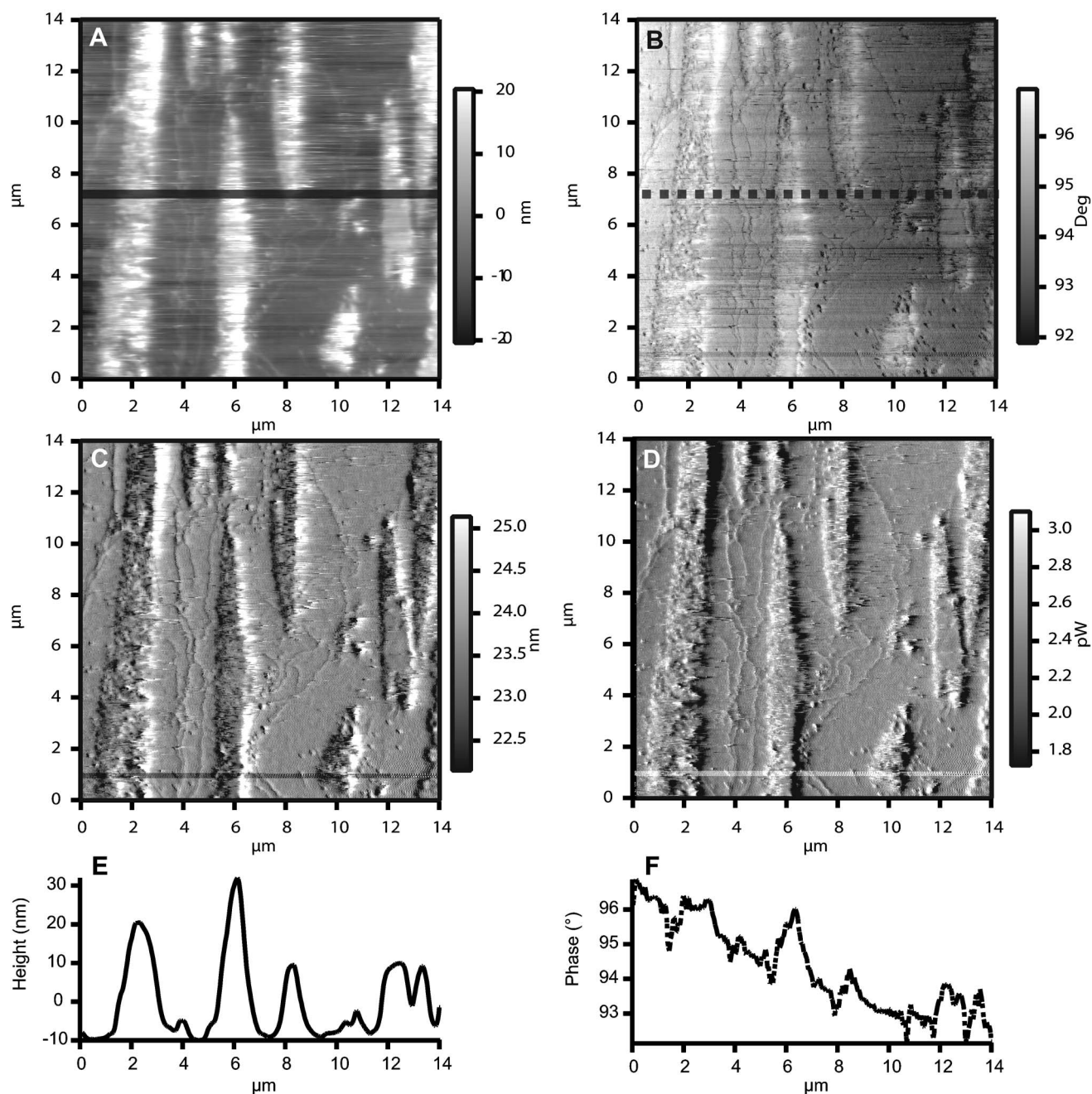


Figure 7. A 15 μm^2 image of an rMSCs acquired by Dynamic Mode AFM. (A) Height trace, (B) amplitude trace, (C) phase trace, (D) energy dissipation. Scan rate 0.5 Hz. For calculation of (D), the dissipation map, $k=1.48$ N m, resonance frequency=28,380 Hz, quality factor=3.9, setpoint amplitude=23.64 nm, drive frequency=27,289 Hz, (E) average height trace of ten scan lines across the cell (F) average phase change of ten scan lines across the cell.

structures emitted higher fluorescence intensity compared to the surrounding F-actin (average normalized fluorescence intensity of six linear F-actin filaments in a single geodesic unit=100±8.27%: average normalized fluorescence intensity of six vertices in a single geodesic unit=130±4.6%* where * $p=0.002$). As one fluorescent unit of the F-actin fluorophore binds to one F-actin subunit (De La Cruz and Pollard, 1994), these results indicate that in the vertices re-

gions there are significantly more F-actin subunits present, therefore indicating the presence of actin bundles and, hence, a mechanical change in this cellular region. We therefore postulate that the increase in relative energy dissipation is mechanical. This result supports the biomechanical model of microfilament tensegrity (soda straw model) and work by Lazarides (1976), which will now be discussed.

Tensegrity is the interaction of a set of interacting discon-

tinuous compression elements (cables) within a set of continuous tension elements (struts) functioning to provide a stable volume and shape to a given object. Cells have been observed to employ tensegrity with tensional components reported as actin microfilaments and the compression units, microtubules (Ingber *et al.*, 1981). However, as stated by Chen and Ingber (1999) tensegrity structures do not have to have isolated struts and cables in order to be defined as tensegrity structures. The actin microfilaments, as observed in this study, can employ a tensegrity design, meaning that the actin microfilaments can function as compression units and tensional components. The microfilament tensegrity system is like no other in that it uses ATP in conjugation with actomyosin filament sliding to generate tension within the cell, hence generating changes in cell morphology. Supporting our observations, Lazarides (1976) reported that the actin vertices do not contain tropomyosin or myosin while the actin fibers extending from the vertices contained α -actinin and tropomyosin. Lazarides (1976) postulated that the vertices could therefore be more flexible than the connecting struts. Lazarides (1976) postulated that this flexible configuration and its interaction with α -actinin in the surrounding actin filaments forms nucleation centers for the outward polymerization of actin filaments. Interestingly, Ingber (1993) stated that the tensegrity model predicts that the tightly packed domes will remodel into long bundles if the pattern of tensile transmission becomes axial. Drawing together information from the observations of Lazarides (1976), the microfilament tensegrity model, the dissipation map and the fluorescence microscopy, we postulate that the vertices act as flexible (compression) units. However, it should also be noted that because the struts are stiff, they could be excited by the cantilever's motion over their length, hence resulting in the observed high dissipation at the vertices, as a result of the cytosol damping the motion of the struts. This effect would become more significant at the junction, where the tip actually excites six struts simultaneously.

Using techniques like dynamic AFM and combined fluorescence microscopy permits the exploration of the mechanical properties of single cells *in situ* under physiological conditions as a function of time and on an array of cell substrates. By developing and evaluating models for the basic principles of cell structure and corresponding mechanics as a product of the interaction with the extracellular matrix a better understanding of cell morphology and phenotype is achievable. This will lead to a better understanding of how to control many physiological and pathological processes by tailoring the cell-substrate interaction.

ACKNOWLEDGMENTS

This work was funded by Science Foundation Ireland (SFI) through the CSET grant at the Centre for Research on Adaptive Nanostructures and Nanodevices (CRANN) and by SFI research Grant No. 00/PI. 1/C028. This work was also partly

funded by the Higher Education Authority (HEA) as part of the Programme for Research in Third Level Institutions (PTRL).

REFERENCES

- Anczykowski, B, Gotsmann, B, Fuchs, H, Cleveland, JP, and Elings, VB (1999). "How to measure energy dissipation in dynamic mode AFM." *Appl. Surf. Sci.* **40**, 376–382.
- Binnig, G, Quate, CF, and Gerber, C (1986). "Atomic force microscope." *Phys. Rev. Lett.* **56**, 930–933.
- Burder, SP, Jaiswal, N, and Haynesworth, SE (1997). "Growth, kinetics, self-renewal and the osteogenic potential of purified human mesenchymal stem cells during extensive subcultivation and following cryopreservation." *J. Cell. Biochem.* **64**, 278–294.
- Chen, CS, and Ingber, DE (1999). "Tensegrity and mechanoregulation: From skeleton to cytoskeleton." *Osteoarthritis Cartilage* **7**, 81–94.
- Chon, JWM, Mulvaney, P, and Sader, JE (2000). "Experimental validation of theoretical models for the frequency response of atomic force microscope cantilever beams immersed in fluids." *J. Appl. Phys.* **87**, 3978–3988.
- De La Cruz, E, and Pollard, TD (1994). "Transient kinetic analysis of rhodamine phalloidin binding to actin filaments." *Biochemistry* **33**, 14387–14392.
- Deroanne, CF, Lapiere, CM, and Nusgens, BV (2001). "In vitro tubulogenesis of endothelial cells by relaxation of the coupling extracellular matrix cytoskeleton." *Cardiovasc. Res.* **49**, 647–658.
- Engler, AJ, Sens, S, Sweeney, HL, and Discher, DE (2006). "Matrix elasticity directs stem cell lineage specification." *Cell* **126**, 677–689.
- Friedenstein, AJ, Gorskaja, U, and Kalugina, NN (1976). "Fibroblast precursors in normal and irradiated mouse hematopoietic organs." *Exp. Hematol.* **4**, 267–274.
- Fuller, B (1965). "Conceptuality of fundamental structures," in *Structure in Art and in Science*, G Kepes (ed.), pp 66–88, Braziller, New York.
- Hayashi, K, and Imai, Y (1997). "Tensile property of atheromatous plaque and an analysis of stress in atherosclerotic wall." *J. Biomech.* **30**, 573–579.
- Henderson, E, Haydon, PG, and Sakaguchi, DS (1992). "Actin filament dynamics in living glial cells imaged by atomic force microscopy." *Science* **257**, 1944–1946.
- Heuser, JE, and Kirschner, MW (1980). "Filament organization revealed in platinum replicas of freeze-dried cytoskeletons." *J. Cell Biol.* **86**, 212–234.
- Higgins, MJ, Proksch, R, Sader, JE, Polick, M, McEndoo, S, Cleveland, JP, and Jarvis, SP (2006). "Noninvasive determination of optical lever sensitivity in atomic force microscopy." *Rev. Sci. Instrum.* **77**, 013701–023705.
- Hofmann, U, Rotsch, C, Parak, WJ, and Ramacher, M (1997). "Investigating the cytoskeleton of chicken cardiocytes with atomic force microscopy." *J. Struct. Biol.* **119**, 84–91.
- Ingber, DE (1993). "Cellular Tensegrity: Defining new rules of biological design that govern the cytoskeleton." *J. Cell. Sci.* **104**, 613–627.
- Ingber, DE, and Jamieson, JD (1985). "Cells as tensegrity structures: Architectural regulation of histodifferentiation by physical forces transduced over basement membrane." in *Gene Expression During Normal and Malignant Differentiation*, LC Andersson, CG Gahmberg, and P Ekblom (eds.), pp 13–32. Academic, Orlando, FL.
- Jiang, W, Ma, J, Wang, T, Han, K, Liu, Y, Zhang, Y, Dong, A, Du, Y, Huang, X, Wang, J, Lei, X, and Zheng, X (2006). "Homing and differentiation of mesenchymal stem cells delivered intravenously to ischemic myocardium in vivo: A time series study." *Eur. J. Physiol.* **453**, 43–52.
- Kici, A, Shen, WY, Wilson, AS, Constable, IJ, Robertson, and Rakoczy, PE (2003). "Differentiation of marrow stromal cells into photoreceptors in the rat eye." *J. Neurosci.* **23**, 7742–7749.
- Lazarides, E (1976). "Actin, α -actinin and tropomyosin interactions in the structural organization of actin filaments in nonmuscle cells." *J. Cell*

- Biol.* **68**, 202–219.
- Lazarides, E, and Weber, K (1974). “Actin antibody: The specific visualization of action filaments in non muscle cells.” *Proc. Natl. Acad. Sci. U.S.A.* **71**(1), 2268–2272.
- Lim, JY, Hansen, JC, Siedlecki, CA, Runt, J, and Donahue, HJ (2005). “Human foetal osteoblastic cell response top polymer-demixed nanotopographic interfaces.” *J. R. Soc., Interface* **2**, 97–108.
- Lo, CM, Wang, HB, Dembo, M, and Wang, YI (2000). “Cell movement is guided by the rigidity of the substrate.” *Biophys. J.* **79**, 144–152.
- Matsumoto, T, Hironobu, A, Ohashi, T, Kato, Y, and Sato, M (2002). “Local elastic modulus of the atherosclerotic lesions of rabbit thoracic aortas measured by pipette aspiration method.” *Physiol. Meas* **23**, 635–648.
- Miller, K, and Theiss, C (2005). “Atomic force microscopy and confocal laser scanning microscopy on the cytoskeleton of peremobilized and embedded cells.” *Ultramicroscopy* **106**, 320–325.
- Nagao, E, and Dvorak, JA (1999). “Phase imaging by atomic force microscopy: analysis of living homoeothermic vertebrate cells.” *Biophys. J.* **76**, 3289–3297.
- Osborn, M, Born, T, Koitsch, H-J, and Weber, K (1978). “Stereo immunofluorescence microscopy: I. Three dimensional arrangement of microfilaments, microtubules, and tonofilaments.” *Cell* **14**, 477–488.
- Pelham, JR, and Wang, YL (1997). “Cell location and focal adhesion are regulated by substrate flexibility.” *Proc. Natl. Acad. Sci. U.S.A.* **94**, 13661–13665.
- Pittenger, MF, Mackay, AM, Beck, SC, Jaiswal, RN, Douglas, R, Mosca, JD., Moorman, MA, Simonetti, DW, Craig, S, and Marshak, DR (1999). “Multilineage potential of adult human mesenchymal stem cells.” *Science* **284**, 143–147.
- Radmacher, M, Cleaveland, JP, Fritz, JP, Hansma, HG, and Hansma, PK (1994). “Mapping interaction forces with the atomic force microscope.” *Biophys. J.* **66**, 2159–2165.
- Sader, JE (1998). “Frequency response of cantilever beams immersed in viscous fluids with applications to the atomic force microscope.” *J. Appl. Phys.* **84**, 64.
- Smolewski, P, Grabarek, J, Hallicka, HD, and Darzynkiewicz, Z (2002). “Assay of caspase activation in situ combined with probing plasma membrane integrity to detect three distinct stages of apoptosis.” *J. Immunol. Methods* **265**, 111–121.
- Sniadecki, R, Desai, R, Ruiz, SA., and Chen, CS (2006). “Nanotechnology for cell-substrate interactions.” *Ann. Biomed. Eng.* **34**, 59–74.
- Takai, E, Coasta, KD, Shaheen, A, Hung, CT, and Guo, XE (2005). “Osteoblast elastic modulus measured by atomic force microscopy is substrate dependent.” *Ann. Biomed. Eng.* **33**, 963–971.
- Takai, E, Landesberg, R, Katz, RW., Hung, CT, and Guo, XE (2006). “Substrate modulation of oesblasts adhesion strength, focal adhesion, kinase activation and responsiveness to mechanical stimuli.” *Mol. Cell Biomech.* **3**, 1–12.
- Wang, YL, and Pelham, RJ (1998). “Preparation of a flexible porous polyacrylamide substrate for mechanical studies of cultures cells.” *Methods Enzymol.* **298**, 489–496.
- Wieland, T (1986). Phallotoxins, Springer-Verlag, New York.
- Wong, JY, Leach, JB, and Brown, XQ (2004). “Balance of chemistry, topography and mechanics at the cell bio-materials interface: Issue and challenges for assessing the role of substrate mechanics on cell responses.” *Surf. Sci.* **570**, 119–133.